



Cite this: *Chem. Commun.*, 2024, 60, 9749

Received 27th May 2024,
Accepted 8th July 2024

DOI: 10.1039/d4cc02570a

rsc.li/chemcomm

Tetraphenylpentalenide organolanthanide complexes†

Nicholas J. Katzer,^{†‡ab} Mandeep Kaur,^{†‡c} Asmita Sen,^{†‡d} Rupal Nimaiyar,^a
Jochen Autschbach,^{†‡d} Polly L. Arnold^{†‡ab} and Ulrich Hintermair^{†‡c}

The D_{2h} symmetrical 1,3,4,6-tetraphenylpentalenide is an excellent ligand for the stabilisation of strongly coloured bis(pentalenide) Ln^{III} sandwich complexes. These easily accessible compounds complement previously reported lanthanide organometallics and provide new opportunities to understand the roles of the f-orbitals in electronic structure and bonding.

Organometallic complexes have made major contributions to the understanding of electronic structure and bonding across the periodic table. Sandwich molecules such as ferrocene and bis(benzene) chromium have led the way and allowed for applications in organic spintronics and single molecule memory storage.¹ f-block compounds can display fascinating electronic properties at the quantum level including magnetism, Kondo behaviour, and superconductivity.^{2–6} Fundamental studies on f-block complexes with unusual electronic structures can help explain these phenomena, potentially providing transformative breakthroughs for quantum computing and future technologies at the nano-scale.^{7–12} Surprisingly, the range of organometallic ligands with the capacity to form bonding interactions with orbitals of many different symmetries is still small and limited mostly to monocyclic aromatic hydrocarbons such as 6π cyclopentadienide (C_5H_5^- , Cp^-)¹³ and 10π cyclooctatetraenide ($\text{C}_8\text{H}_8^{2-}$, COT^{2-})¹⁴ derivatives.¹⁵ The use of bicyclic 10π pentalenide ($\text{C}_8\text{H}_6^{2-}$, Pn^{2-} ; Fig. 1) in f-block organometallic chemistry has grown in popularity due to its D_{2h} symmetry

allowing for favorable bonding interactions involving δ -symmetry orbitals and the metal's d_{z^2} which are not available in the COT analogues due to their D_{8h} symmetry.¹⁶ Besides the parent Pn^{2-} synthesised by *in situ* deprotonation of unstable dihydropentalene,¹⁷ 1,4-disilylated derivatives (Pn^{\dagger})^{2–} with increased stability and solubility have been reported.¹⁸ A hexamethylated pentalenide (Pn^*)^{2–} can also be accessed by a multi-step organic synthesis,¹⁹ and more recently 1,3,4,6-tetraphenyl pentalenide ($\text{Ph}_4\text{Pn}^{2-}$) has been reported to be accessible through the ring-closing condensation of Cp' s with enones.^{20,21}

Bis(η^8 -pentalenide) sandwich compounds $[\text{M}(\eta^8\text{-C}_8\text{H}_n(\text{R})_{6-n})_2]$ have been reported for Ti, Zr, Hf, Ce, Th, and U.¹⁸ These formal 20 electron complexes typically feature a staggered conformation with some degree of folding of the pentalenide around its bridgehead carbons (CB, $\text{C}_7\text{--C}_8$; Fig. 1).²² We were interested in the f-block chemistry of sandwich structures such as $\text{K}[\text{Ce}^{\text{III}}(\eta^8\text{-Pn}^*)]_2$,²³ and M^{IV} ($\text{M} = \text{Ce}, \text{U}, \text{Th}$) containing $[\text{M}(\eta^8\text{-Pn}^*)]_2$ (Fig. 2),^{24–26} because the ground state electronic structure of cerocene, and also the actinocenes, has been the subject of much debate.²⁷ In particular, comparison of the planar D_{8h} symmetrical COT^{2-} with the folded D_{2h} symmetrical Pn^{2-} in the stabilisation of f-block cations should offer further insight into the covalency in f-block bonding.^{28–30} The ground state electronic structure of $[\text{Ce}(\text{COT})_2]$ is probably best viewed as a mixture of $\sim 80\%$ Ce^{III} with an isolated $4f^1$ cation coupled to an unpaired electron in the rings' π orbitals, and $\sim 20\%$

^a Department of Chemistry, University of California, Berkeley, CA, 94720, USA.

E-mail: pla@berkeley.edu

^b Chemical Sciences Division, Lawrence Berkeley National Laboratory, Berkeley, CA 94720, USA

^c Department of Chemistry, University of Bath, BA2 7AY, UK.

E-mail: u.hintermair@bath.ac.uk

^d Department of Chemistry, University at Buffalo, State University of New York,

Buffalo, NY 14260, USA. E-mail: jochena@buffalo.edu

† Electronic supplementary information (ESI) available: CCDC 2332849, 2357823–2357832. For ESI and crystallographic data in CIF or other electronic format see DOI:

<https://doi.org/10.1039/d4cc02570a>

‡ Equal contributions.

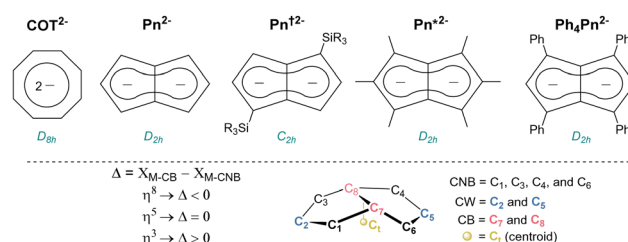


Fig. 1 Dianionic 10π ligands for organometallic complexes (upper) and positional numbering and hapticity definition of pentalenides (lower).





Fig. 2 F-block bis(pentalenide) sandwich complexes (upper) and geometric definitions of relevant structural parameters (lower).

of a state containing the Ce^{IV} ion sandwiched by two aromatic 10π dianions with significant Ce 4f–ring covalency.^{31–33} Pentalenides have also been shown to support pianostool f-block complexes with interesting properties. For example, $[(\eta^8\text{-Pn}^+)\text{Dy}^{\text{III}}(\eta^5\text{-Cp}^*)]$ behaves as a single molecule magnet with an energy barrier of 245 cm^{-1} .³⁴ In related U^{III} complexes the fold of the Pn^{2-} ligand was noted as important for subsequent reactivity such as dinitrogen reduction to form $(\text{N}_2)[\text{U}(\eta^5\text{-Cp}^*)(\eta^8\text{-Pn}^+)]_2$.^{35,36}

Here we explore the organometallic lanthanide chemistry of 1,3,4,6-tetraphenylpentalenide $\text{Ph}_4\text{Pn}^{2-}$ with a range of 4f cations and study the metal–ligand bonding both experimentally and computationally.

Salt metathesis reactions between dilithium, disodium, or dipotassium salts of $\text{Ph}_4\text{Pn}^{2-}$ reacted cleanly with half an equivalent of anhydrous lanthanide(III) halides in THF or DME to afford the pentalenide Ln sandwich ‘ate’ complexes $[\text{M}(\text{sol})_m][\text{Ln}^{\text{III}}(\text{Ph}_4\text{Pn})_2]_2$ (**1-Ln**) for Ln = Y (orange), La (bright orange), Ce (rust-orange), Tb (bright red), Yb (red-orange) (Scheme 1). These are a good representation of the size and Lewis acidity range for the rare earths, with $r_{\text{covalent}}(\text{6-coordinate Ln}^{\text{III}}) = 0.900\text{ \AA}$ (Y), 1.032 \AA (La), 1.01 \AA (Ce), 0.923 \AA (Tb),

0.868 (Yb) .³⁷ The reactions proceed most cleanly for the largest Ln, with isolated yields of 76% for **1-La**, 87% for **1-Ce**, and 77% for **1-Tb**, but only a few single crystals could be isolated from the reaction that afforded **1-Yb**. ^1H NMR spectroscopic analysis of the crude product solution of the latter suggested the formation of a mixture of products, so further efforts to isolate pure material were not pursued. We have also crystallographically characterized the new DME adducts of $\text{Li}_2[\text{Ph}_4\text{Pn}]$, $\text{K}_2[\text{Ph}_4\text{Pn}]$, and **1-Ln** (Fig. S12 and S22, ESI†).

Magnesium pentalenides may also be used to make rare earth pentalenide sandwich complexes.³⁸ A metathesis reaction between $\text{Mg}[\text{Ph}_4\text{Pn}]$ and $\text{Y}(\text{N}^{\text{R}})_3$ ($\text{N}^{\text{R}} = \text{bis}[\text{trimethylsilyl}]\text{amide}$, Scheme 1) gave the magnesium congener of **1-Y**, orange $[\text{Mg}(\text{THF})_5][\text{Y}^{\text{III}}(\text{Ph}_4\text{Pn})_2]_2$ (**2**) in 40% isolated yield plus $\text{Mg}(\text{N}^{\text{R}})_2$ as a by-product. An orange slurry of equimolar YCl_3 and $\text{Mg}[\text{Ph}_4\text{Pn}]$ in THF at room temperature immediately turns red, and work-up after four hours yields the trimetallic $[(\text{Mg}^{\text{II}})_2\text{Y}^{\text{III}}]$ halide bridged complex $[\text{MgCl}(\text{THF})_5][(\text{Y}^{\text{III}}\text{Ph}_4\text{Pn})_2(\mu\text{-Cl})_5\text{Mg}(\text{THF})_4]$ (**3**, Scheme 1). The same reaction with group 1 pentalenide salts gave similar results (Fig. S1, ESI†), suggesting the formation of halide-bridged mono-pentalenide clusters to be characteristic of the harder Y^{III} cation.³⁹ Attempts to break up the halide bridges to access monomeric pianostool Y^{III} complexes by addition of AgPF_6 , $\text{B}(\text{C}_6\text{F}_5)_3$, or AlCl_3 led to decomposition into unidentifiable mixtures, but **3** could be converted to the bis(pentalenide) sandwich $[\text{Mg}(\text{THF})_5][\text{Y}^{\text{III}}(\text{Ph}_4\text{Pn})_2]_2$ (**2**) congener to **1-Y** by addition of dioxane, as confirmed by NMR and XRD (Fig. S2, ESI†). All these reactions support the expectation that the bis- η^8 sandwich complexes are the thermodynamically favored products for the rare earth cations.

The ^1H NMR spectra of the diamagnetic **1-Ln** and **2** show diagnostic resonances for the pentalenide wingtip protons H_w which are sensitive reporters for the degree of shielding of the 10π system (Fig. 1).⁴⁰ Spectra of **1-La** in THF show a single resonance for the two equivalent H_w at 6.39 ppm and a corresponding C_w resonance at 122.5 ppm. Comparatively, the NMR spectra of **2** in THF contained a single ^1H resonance for H_w at 7.20 ppm and a ^{13}C resonance for C_w at 124.1 ppm. The latter is 8.6 ppm higher frequency than in $\text{Mg}[\text{Ph}_4\text{Pn}]$ which exists as a solvent-separated ion pair in ethereal solution.³⁸ The NMR spectra of the cluster complex **3** also show a D_{2h} symmetrical pentalenide with one sharp set of equivalent H_w at temperatures down to $-60\text{ }^\circ\text{C}$ in THF, while DOSY analysis suggests the cluster anion of **3** remains intact in solution ($D = 6.325 \times 10^{-10}\text{ m}^2\text{ s}^{-1}$ corresponding to 1462 g mol^{-1} compared to $\text{MW} = 1484\text{ g mol}^{-1}$; Fig. S3, ESI†). These observations support the presence of strong Mg–Cl–Y interactions in the trinuclear cluster with rapid ring slippage of the η^5 pentalenide on Y^{III} .⁴¹

The D_{2h} symmetry of 1,3,4,6- $\text{Ph}_4\text{Pn}^{2-}$ greatly facilitates structural analysis of the new sandwich complexes in solution and in the solid state, as it eliminates the formation of *meso*, *rac*, and twist isomers seen with the C_{2h} symmetrical 1,4-bis(silyl)-substituted $(\text{Pn}^+)^{2-}$ (Fig. 1).¹⁸ **1-Ln** crystallize as either solvent-separated ion pairs (SSIP) or contact ion pairs (CIP) depending on the solvent and counteraction. In each case, the Ln^{III} ion sits on a crystallographic C_2 axis positioned centrally



Scheme 1 Synthesis of $[\text{M}(\text{sol})_m][\text{Ln}^{\text{III}}(\text{Ph}_4\text{Pn})_2]_2$ (**1-Ln**) for Ln = Y, La, Ce, Tb, Yb from group 1 pentalenide salts (for Ln = Y, M = Li, $n = 4$, X = Cl, sol = THF, $\text{M}(\text{sol})_m = \text{Li}(\text{DME})_3$; for Ln = Ce, M = K, $n = 2$, X = Br, sol = DME, $\text{M}(\text{sol})_m = \text{K}(\text{DME})_4$; for Ln = Yb, M = Na, $n = 6$, X = Cl, sol = THF, $\text{M}(\text{sol})_m = \text{Na}(\text{THF})_5$), synthesis of the Mg analogue of **1-Y**, $[\text{Mg}(\text{THF})_5][\text{Y}^{\text{III}}(\text{Ph}_4\text{Pn})_2]_2$ (**2**) from a magnesium pentalenide, and a half-sandwich cluster $[\text{MgCl}(\text{THF})_5][(\text{Y}^{\text{III}}\text{Ph}_4\text{Pn})_2(\mu\text{-Cl})_5\text{Mg}(\text{THF})_4]$ (**3**).

between two parallel (C_t -Ln- C_t angles close to 180°) but staggered $\text{Ph}_4\text{Pn}^{2-}$ ligands which are rotated by 38 – 76° against each other with noticeable inward folding by $\sim 24^\circ$ to form a hydrocarbon capsule around the metal.²⁴ Each C_5 ring of the pentalenide remains planar with no noticeable wingtip hinging, and phenyl twist angles are in the typical range of 19 – 49° previously observed for other s- and d-block complexes of $\text{Ph}_4\text{Pn}^{2-}$.^{20,38,41} Ring slippage values of $\Delta = -0.3$ indicate bis- η^8 coordination for all metals and M- C_t distances are similar once normalized for the metal radius, except for **1-Yb** where the M- C_t of 2.280 \AA is anomalously long, and **2** where the M- C_t of 2.048 \AA is anomalously short. Both of these also have larger pentalenide rotation angles of 76.2 and 71.9° respectively, compared to an average of 38.6° for the others. **1-Ce(DME)** is shown in Fig. 3 (left) as an example. The solid-state structure of complex **3** (Fig. 3, right) can be considered to comprise two $[\text{Y}^{\text{III}}(\text{Ph}_4\text{Pn})\text{Cl}_2]^-$ anions linked by a $[\text{MgCl}]^+$ cation through bridging halides, with THF molecules saturating the coordination spheres of Mg^{II} and Y^{III} . In contrast to **1** and **2**, in **3** the $\text{Ph}_4\text{Pn}^{2-}$ ligands bind to each Y^{III} in nearly perfect η^5 coordination ($\Delta = -0.006$). The 2.319 \AA Y- C_t distance in **3** is significantly longer than that in **2** (2.048 \AA), consistent with lower hapticity and thus weaker binding.

Starting from the crystal structure data, molecular geometries were optimised computationally for $[\text{Ln}^{\text{III}}(\eta^8\text{-Ph}_4\text{Pn})_2]^-$ with Ln = La, Ce, and Tb in their respective electronic ground states with $S = 0, \frac{1}{2}, 3$ using the PBE0 functional (see ESI† for details).^{42–44} All structures were confirmed as minima *via* harmonic vibrational frequency calculations, and all Ln-C distances agreed very well with those found experimentally (Fig. S23–S25, S30 and Tables S1–S3, S9–S11, ESI†). Superimposing the optimized geometries on the crystal structures showed the latter to be representative of what would likely be found in solution (as obtained from the calculations; see Fig. S26 and Table S4, ESI†). The chemical bonding and metal electronic configurations were analysed by Natural Localized Molecular Orbitals (NLMOs) and Natural Population Analysis (NPA). Each ligand has a 10-electron 5-orbital π system in the bicyclic core represented by ligand-centred NLMOs that are strongly delocalized over the pentalenide (as is typical for delocalized π -donor ligands)⁴⁰ and clearly donating electron density to the metal. For example, the ten (both ligands) relevant **1-La** NLMOs each contain 3–5% La character, which

sums to about 0.24/0.57 electrons being donated to 4f/5d and the remainder into more diffuse shells (Table S5, ESI†). At La, these NLMOs are mainly of 5d character ($> 50\%$) with secondary 4f admixtures (Fig. S27, ESI†). The La charge as determined by NPA is +1.85, smaller than the formal +3 charge, as expected because of ligand to metal electron donation. Optimised molecular structural data in comparison with experimental parameters are provided in Tables S1–S3 (ESI†), along with Ln-C Wiberg bond orders (WBOs). In agreement with a recent suggestion,⁴⁵ the bridgehead carbons, which are closest to the metal, generate the largest WBOs. Similar bonding patterns were found in **1-Ce** and **1-Tb** (Table S5 and Fig. S24–S25, S28 and S29, ESI†) but we note that there is almost no donation into 4f for the Tb system, with the occupancy determined as $4f^{0.24}$, $4f^{1.22}$, and $4f^{8.04}$ for La, Ce, and Tb congeners respectively. The calculations also reveal π -delocalization between the pentalenide core and the phenyl substituents as found earlier for the THF-solvated Li salts,⁴⁰ resulting in reduced ligand-to-metal donation compared to the parent Pn^{2-} (Table S6, ESI†). The overall -1 charge of each complex is balanced by the donation between ligands and the metal, with the eight phenyl groups in each complex collectively holding a charge of about -0.5 (Table S7, ESI†). We also performed comparative calculations for the analogous $[\text{Ln}^{\text{III}}(\eta^8\text{-COT})_2]^-$ complexes (Table S8, ESI†) which show overall the order of ligand-to-metal donation increases from $\text{Ph}_4\text{Pn}^{2-}$ through COT^{2-} to Pn^{2-} , with most of the differences impacting the donation into 5d and more diffuse shells. The extent of donation into 4f is similar for the three types of ligands.

The experimental UV-vis-NIR spectra of **1-La**, **1-Ce** and **1-Tb** in DME are dominated by an intense absorption around 380 nm with extinction coefficients of $> 30\,000 \text{ M}^{-1}\text{cm}^{-1}$ (Fig. 4 and Fig. S10, ESI†), whereas for the Y^{III} complexes **2** and **3** in THF these transitions are slightly less intense and blue-shifted by around 30 nm (Fig. S11, ESI†). The spectra of **1-La** and **1-Ce** further feature weaker lower-energy transitions around 550 and 750 nm .



Fig. 3 Molecular structures of (left) the anion of **1-Ce(DME)** and (right) the anionic MgY_2 pentalenide cluster of **3**. Selected ellipsoids drawn at 50% probability; H atoms, counter cations and lattice solvent omitted for clarity.

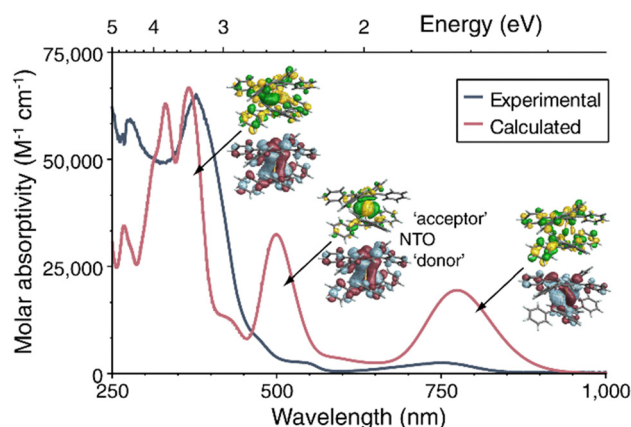


Fig. 4 UV-vis-NIR spectrum of **1-La** in DME at room temperature (dark blue). TD-DFT calculated spectrum (red). Insets: representative NTOs (isosurfaces) for the most intense transitions.



Time-dependent DFT calculations of the electronic excitation spectra of **1-Ln** reproduced the observed spectral patterns in gas phase calculations as well as with the use of a solvent model, although at the chosen level of broadening the computed bands are more intense in the low-energy regions than the experimental spectra (Fig. S31, S33 and S36, ESI†). The natural transition orbital (NTO) analysis of **1-La** (Fig. 4 and Fig. S32, ESI†) shows low-energy bands around 1.6 eV/780 nm and 2.5 eV/500 nm. The calculated spectrum also features comparatively intense bands at energies of 3.1 eV and higher/400 nm and below. According to the NTO analysis, an intense transition calculated around 375 nm has mixed intra-ligand, MLCT, and metal 5d to 6p character, the latter being possible because of the donation into 5d in the ground state. The most intense transition in the 500 nm peak is mixed LMCT and 5d–5d, with the acceptor NTO of the dominant contribution to the transition having approximate δ symmetry about the C_t –Ln– C_t axis. The donor ('hole') NTO in both cases corresponds closely to the HOMO–1. The band at lowest energy is assigned as HOMO to ligand π^* with weak metal contributions in the acceptor NTO (Fig. 4). The peak assignment is qualitatively similar for the corresponding absorptions of **1-Ce** (Fig. S33–S35, ESI†) and **1-Tb** (Fig. S36–S37, ESI†). In contrast to the analogous **COT**^{2–} complexes, participation of the phenyl substituents is clearly noticeable in the NTOs. Furthermore, the pentalenides induce mixing of rotational symmetries of σ , π , δ , and ϕ where the metal and ligand fragment orbitals are similar in energy (Fig. 4 and Fig. S38–S43, ESI†).

In conclusion, the **Ph₄Pn**^{2–} ligand is highly suited for stabilising f-block organometallics giving access to both half-sandwich as well as sandwich complexes of the rare earths. Its ease of synthesis, high symmetry and ready crystallisation facilitate NMR and XRD analysis and promises access to the first homologous series of f-block pentalenide sandwich complexes to investigate fundamental aspects of electronic structure and bonding. In comparison to unsubstituted **Pn**^{2–} and **COT**^{2–} we find **Ph₄Pn**^{2–} to be a better acceptor, *i.e.* the order of ligand-to-metal electron donation (primarily into 5d orbitals) is **Pn** > **COT** > **Ph₄Pn**. This will prove useful for the stabilisation of electron-rich f-block organometallics where the comparatively low symmetry offers positive overlap of ligand frontier orbitals with the metal ion's d_{z²} orbital which is not possible in the **COT**^{2–} complexes.

The synthetic parts of this research were supported by UK's Royal Society (awards URF\R\221049 and RF\ERE\221083), the Heavy Element Chemistry Program and the Molecular Qubits Project of the Quantum Information Science program of the U.S. DOE, Office of Science, Basic Energy Sciences, CSG Division under contract DE-AC02-05CH11231 (PLA). MK and UH thank Dr Gabriele Kociok-Köhn from the Chemical Characterisation Analysis at Bath for XRD analyses. JA acknowledges DOE grant DE-SC0001136 (Heavy Element Chemistry) for supporting the theoretical component of this study. We thank Drs. Hasan Celik, Raynald Giovine, and Pines Magnetic Resonance Center's Core NMR Facility for spectroscopic assistance.

One instrument used in this work was in part supported by NIH S10OD024998 and the PMRC Core. Computations were carried out at the Center for Computational Research at the University at Buffalo (<https://hdl.handle.net/10477/79221>).

Data availability

Crystallographic datasets are available from the CCDC deposition numbers 2332849, 2357823–2357832 and other analytical data can be retrieved via DOI: <https://doi.org/10.5061/dryad.sxksn03bf>.

Conflicts of interest

There are no conflicts of interest to declare.

References

- 1 H. Werner, *Angew. Chem., Int. Ed.*, 2012, **51**, 6052.
- 2 S. Bart and E. Schelter, *Organometallics*, 2017, **36**, 4507.
- 3 L. Ungur and L. Chibotaru, *Inorg. Chem.*, 2016, **55**, 10043.
- 4 C. Gould, *et al.*, *J. Am. Chem. Soc.*, 2019, **141**, 12967.
- 5 N. Mahieu, *et al.*, *Chem. Sci.*, 2023, **14**, 443.
- 6 E. Castellanos and S. Demir, *Inorg. Chem.*, 2023, **62**, 2095.
- 7 L. Münzfeld, *et al.*, *Angew. Chem., Int. Ed.*, 2023, **62**, e202218107.
- 8 P. Arnold, *et al.*, *Nat. Chem.*, 2012, **4**, 668.
- 9 W. Huang, *et al.*, *Nat. Commun.*, 2013, **4**, 1448.
- 10 S. Minasian, *et al.*, *Chem. Sci.*, 2014, **5**, 351.
- 11 D. Smiles, *et al.*, *Chem. Sci.*, 2020, **11**, 2796.
- 12 C. Gould, *et al.*, *Nat. Chem.*, 2021, **13**, 1001.
- 13 P. Jutzi and N. Burford, *Chem. Rev.*, 1999, **99**, 969.
- 14 F. Sroor, *J. Organomet. Chem.*, 2021, **948**, 121878.
- 15 P. Arnold, *et al.*, *Inorg. Chem.*, 2021, **60**, 4162.
- 16 R. King, *Appl. Organomet. Chem.*, 2003, **17**, 393.
- 17 T. Katz and N. Acton, *J. Am. Chem. Soc.*, 1972, **94**, 3281.
- 18 F. Cloke, *et al.*, *Coord. Chem. Rev.*, 2017, **344**, 238.
- 19 A. Ashley, A. Cowley and D. O'Hare, *Chem. Commun.*, 2007, 1512.
- 20 S. Boyt, *et al.*, *Organometallics*, 2022, **41**, 211.
- 21 N. Jenek, *et al.*, *J. Org. Chem.*, 2022, **87**, 13790.
- 22 K. Costuas and J.-Y. Saillard, *Chem. Commun.*, 1998, 2047.
- 23 A. Ashley, *et al.*, *Chem. Commun.*, 2007, 1515.
- 24 G. Balazs, *et al.*, *Organometallics*, 2007, **26**, 3111.
- 25 O. Summerscales and F. Cloke, *Coord. Chem. Rev.*, 2006, **250**, 1122.
- 26 F. Cloke and P. Hitchcock, *J. Am. Chem. Soc.*, 1997, **119**, 7899.
- 27 O. Walter in *Comprehensive Organometallic Chemistry IV*, Elsevier, 2022, p. 582.
- 28 M. Neidig, D. Clark and R. Martin, *Coord. Chem. Rev.*, 2013, **257**, 394.
- 29 A. Kerridge, *Chem. Commun.*, 2017, **53**, 6685.
- 30 S. Cooper and N. Kaltsoyannis, *Dalton Trans.*, 2021, **50**, 1478.
- 31 D.-C. Sergentu, *et al.*, *Chem. Eur. J.*, 2021, **27**, 7239.
- 32 O. Moosén and M. Dolg, *Chem. Phys. Lett.*, 2014, **594**, 47.
- 33 G. Ganguly, *et al.*, *Chem. Eur. J.*, 2020, **26**, 1776.
- 34 A. Kilpatrick, *et al.*, *Chem. Commun.*, 2018, **54**(51), 7085.
- 35 F. Cloke and P. Hitchcock, *J. Am. Chem. Soc.*, 2002, **124**, 9352.
- 36 N. Tsoureas, *et al.*, *J. Am. Chem. Soc.*, 2020, **142**, 89.
- 37 R. Shannon, *Acta Crystallogr., Sect. A: Found. Crystallogr.*, 1976, **32**, 751.
- 38 H. Sanderson, *et al.*, *Inorg. Chem.*, 2023, **62**, 15983.
- 39 R. Cooper, *et al.*, *Organometallics*, 2013, **32**, 2228.
- 40 N. Jenek, *et al.*, *Chem. Sci.*, 2024, DOI: [10.1039/D3SC04622B](https://doi.org/10.1039/D3SC04622B).
- 41 H. Sanderson, *et al.*, *Dalton Trans.*, 2024, **53**, 5881.
- 42 E. Glendening, *et al.*, *Wiley Interdiscip. Rev.: Comput. Mol. Sci.*, 2012, **2**, 142.
- 43 C. Adamo and V. Barone, *Chem. Phys. Lett.*, 1998, **298**, 113.
- 44 E. Baerends, *et al.*, *Amsterdam Density Functional (ADF) program*, Version 2023.104.
- 45 E. Reinhart, *et al.*, *Organometallics*, 2024, **43**, 284.

